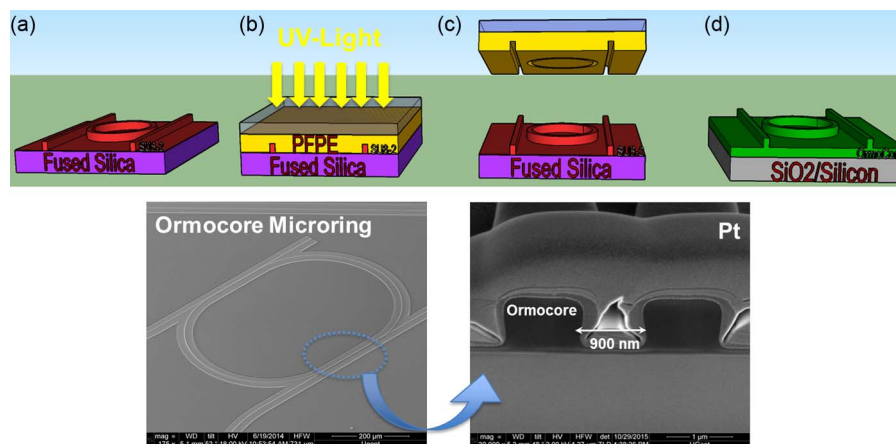


Fabrication and Characterization of High-Optical-Quality-Factor Hybrid Polymer Microring Resonators Operating at Very Near Infrared Wavelengths

Volume 8, Number 2, April 2016

R. Morarescu
P. K. Pal
N. T. Beneitez
J. Missinne
G. V. Steenberge, Senior Member, IEEE
P. Bienstman, Senior Member, IEEE
G. Morthier, Senior Member, IEEE



DOI: 10.1109/JPHOT.2016.2544641
1943-0655 © 2016 IEEE

Fabrication and Characterization of High-Optical-Quality-Factor Hybrid Polymer Microring Resonators Operating at Very Near Infrared Wavelengths

R. Morarescu,^{1,2} P. K. Pal,^{1,2} N. T. Beneitez,³ J. Missinne,³
G. V. Steenberge,³ *Senior Member, IEEE*,
P. Bienstman,^{1,2} *Senior Member, IEEE*, and
G. Morthier,^{1,2} *Senior Member, IEEE*

¹Photonics Research Group, Department of Information and Technology,
Ghent University, Ghent 9000, Belgium

²Center for Nano- and Biophotonics (NB-Photonics), Ghent University, Ghent 9000, Belgium

³Centre for Microsystems Technology (CMST), IMEC and Ghent University, Ghent 9052, Belgium

DOI: 10.1109/JPHOT.2016.2544641

1943-0655 © 2016 IEEE. Translations and content mining are permitted for academic research only.

Personal use is also permitted, but republication/redistribution requires IEEE permission.

See http://www.ieee.org/publications_standards/publications/rights/index.html for more information.

Manuscript received March 1, 2016; accepted March 16, 2016. Date of publication March 21, 2016; date of current version April 7, 2016. This work was supported by Research Foundation—Flanders (FWO) under Grant G.0533.13N (2013–2015). Corresponding author: R. Morarescu (e-mail: Rodica.Morarescu@intec.ugent.be).

Abstract: In this paper, we present a new fabrication method for large-area hybrid polymer microring resonators using a rib waveguide configuration with a minimum residual layer down to 40 nm by ultraviolet (UV) nanoimprint lithography. In a first step, a negative photoresist (SU8-2) patterned by photolithography on an SiO₂/silicon wafer was used as a master mold. Flexible soft molds using perfluoropolyether (PFPE)-based elastomers for high-resolution replica molding are explored in the imprinting process flow. High-quality devices with Q -factors up to 39000 and finesses up to $F \sim 14$ were demonstrated for very-near infrared wavelengths (around 900 nm). Finally, we report that the resonances can be thermo-optically tuned by 0.05 nm/°C at 896 nm, thus demonstrating that, at shorter wavelengths, the fabricated microring resonators are less sensitive to temperature change, compared with longer wavelengths. The results of this paper demonstrate the capability of our method to fabricate optical devices with high performance for operation in a single mode at wavelengths where cheap light sources are available and water absorption is much lower than at far-infrared wavelengths. Because of this, it is expected that the fabricated structures have high potential for biosensing applications.

Index Terms: Hybrid polymer photonic device, ultraviolet (UV) nanoimprint, optical waveguides, racetrack microring resonator.

1. Introduction

Polymer materials have garnered significant interest over the past few years among both academia and industry since they may open new avenues toward fabrication of discrete photonics components and integrated optical devices. Obviously, this is because of their extraordinary properties, with, most importantly, high optical transmittance, but an easier fabrication process,

flexibility, and their potential for low-cost production as well [1], [2]. Regarding the fabrication of polymer devices, different methods have been described in the literature so far, e.g., photolithography, electron beam lithography, excimer laser micromachining [3], [4]. Among them, nanoimprint lithography (NIL) has become increasingly popular during the last decade [5], [6]. It has been developed as a cost-effective alternative patterning technology and to overcome the resolution limitations of standard photolithography. It has been reported that NIL with low-cost equipment can fabricate high-resolution nanopatterns down to sub-25 nm resolution on a large scale with a high repeatability [7]. NIL, unlike traditional lithographic processes, is based on the mechanical deformation of the polymer layer using a mold to define the structures [8]–[10]. This replication technology is either thermal or UV-based and can be used on various types of substrates. After the imprinting and the demolding steps, the patterns of the mold are copied in the desired polymer. A crucial requirement in the imprinting process is the mold choice which can be either “hard” or “soft,” and this choice depends on the polymer’s physical properties, chemical composition and moreover on the desired imprinted pattern. Additionally, for imprinting with hard molds (e.g. silicon, fused silica), several issues such as the need for imprinting under vacuum using large force, have to be considered in order to overcome a non-uniform imprint and avoid the damage and deformation of the generated pattern. To overcome this issue, replica molding utilizing soft molds has gained increasing interest recently and it is the chosen method for this study. With this technique, new device architectures become feasible with a limited number of process steps, and moreover with a high accuracy, repeatability and low cost [11]. So far, a wide variety of materials have been developed to improve soft mold performance. The primary and the most popular elastomer for nanofabrication is polydimethylsiloxane (PDMS). Although PDMS generally emerged as a material of choice for soft lithography, there are several drawbacks that limit the feature size and aspect ratio that can be replicated. In order to overcome the drawbacks associated with the use of PDMS, research efforts have resulted in the discovery of new polymeric stamps with increased resolution and material compatibility. Among them, the use of fluorinated elastomers opens an attractive route for nanoimprint lithography [12]. The DeSimone laboratory pioneered the use of photocurable perfluoropolyether-based (PFPE) materials as an alternative to PDMS for soft lithography applications [13]. It is well known that the Young’s modulus, surface free energy and the surface tension of the mold material will affect the resolution of the imprinted pattern. In choosing a material for the soft molds, we have to consider that its Young modulus should be sufficiently high and the surface free energy should stay as low as possible.

The motivation of our work was to fabricate large areas of microring resonators (MRRs) with a minimum number of process steps operating in the very-near infrared region (around 900 nm). Our optimized fabrication method results in generation of patterns with a minimum residual layer of 40 nm without an etching step. The bend loss decreases significantly with decreasing thickness of the residual layer and consequently this increases the Q -factor. Considerable work on polymer optical devices at infrared wavelengths has been reported [14]. However, there is an urgent challenge and demand for the development of polymer photonic based device closer to/ or at visible wavelengths where the absorption of water is about 2000 times lower than in near infrared regions and lower cost light sources are available in this range [15]. In this work, we are exploring two PFPE materials, i.e., Fluorolink MD 700 (Solvay Solexis) and Fomblin MD 40 (Solvay Solexis) for the fabrication of a soft mold on a flexible polystyrene substrate. We compare the devices fabricated with these materials, and we optically characterized their performance. The devices fabricated with MD 700 demonstrate higher Q -factors due to the lower bend losses. Finally, we thermo-optically tuned the MRR resonances, demonstrating that at shorter wavelengths, the MRRs are less sensitive to temperature changes compared to longer wavelengths.

2. Device Fabrication: Method and Results

In order to estimate the resonator parameters for good performance at the wavelength $\lambda = 890$ nm, in a first step prior to the design and physical fabrication of the resonators,

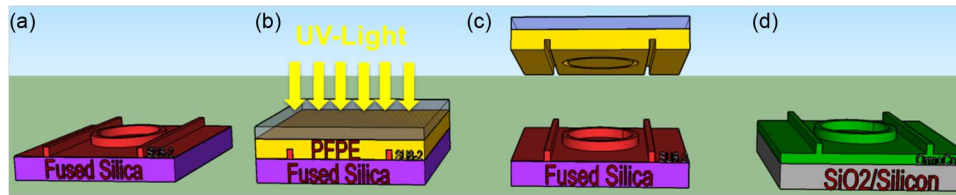


Fig. 1. Schematic of the fabrication process of microring resonators. (a) SU8 master mould has been prepared by photolithography. (b) Formation of the soft mold: PFPE casting on the top of master mold and UV curing. (c) Soft mold is peeled off from the master mold. (d) Generation of the Ormocore WGs by UV-NPL.

simulations with the commercial Fimmwave software [16] have been performed and were reported in previous work [17]. As a core material we used the hybrid polymer Ormocore [18] with a high refractive index of $n_{\text{core}} = 1.543$. Silicon wafers are used as substrates with a $3 \mu\text{m}$ thermal oxide on the top which act as cladding ($n_{\text{cladding}} = 1.453$). As the number of guided modes depends of the waveguide geometry, initially it has been determined that for single-mode operation at 890 nm, the waveguide width and height, within a range of dimension tolerances, can be fixed to $1 \mu\text{m}$. Thanks to the racetrack configuration of the add-drop microrings used in this study, we maintain the optical performance of the structure while extending the tolerance range of the fabrication process by increasing the values of the gap to around 900 nm. The coupling length is $190 \mu\text{m}$. Microrings with high Q -factors are desired for many applications, including biosensing. Low losses will lead to higher Q -factors; therefore, in the fabrication process, any kind of loss should be minimized. As already mentioned, the MRR structures were prepared in our cleanroom using a nanoimprint technique. This etch-free process flow is schematically depicted in Fig. 1.

In a first step, a negative photoresist (SU8-2 from MicroChemicals) was patterned by photolithography (see Fig. 1(a)). Due to its unique physical, chemical and mechanical properties, SU8-2 has been explored for the fabrication of the master mold. First, promotion of adhesion of SU8-2 on fused silica was done by spin-coating of Ti-primer (MicroChemicals) at 3000 rpm for 40 seconds. After SU8-2 was spun on fused silica at 5600 rpm for 40 seconds and baking steps were performed, it was exposed using the contact mask aligner Süss MA6 to UV light through a chromium mask. The SU-8 film thickness was about 960 nm. After the development of the resist, in which the unexposed part of SU8-2 was removed, the substrates were hard-baked at $180 \text{ }^\circ\text{C}$ for 3 minutes in order to decrease the surface roughness. In the past, it has been demonstrated that the thermal reflow method gives efficiently smooth sidewall waveguides [19]. The exposure, the development time, as well as the baking and the flood exposure time have been optimized in order to generate structures with a very good quality. This quality of the master mold, including its surface roughness, is essential in the replication process where all the patterns are imprinted in the desired polymer, including the defects. After the master mold fabrication, the PFPE acrylate composite molds were prepared by thoroughly mixing 3% Irgacure 2022 photoinitiator (BASF) to Fomblin MD 40 (Solvay Solexis) and Fluorolink MD 700 (Solvay Solexis), respectively. Afterwards, these mixtures were cast on top of the SU8 master mold [see Fig. 1(b)] Polystyrene foils were placed on the top for mechanical stability of the soft mold. UV-light was used to cure the PFPE material for 1 min with an intensity of 30 mW/cm^2 . As depicted in Fig. 1(c) peeling off the composite PFPE mold from the SU8-2 master mold completed the soft mold formation. One of the advantages of the proposed method is that there is no need to treat the master mold with an antiadhesive coating. Both molds prepared using MD 40 and MD 700 were used for the imprinting in the Ormocore material. The final imprinting processes started with the preparation of thin Ormocore films on a SiO_2 insulator on Si substrate preliminary cleaned and dehydrated. The $3 \mu\text{m}$ thermal oxide layer is thick enough in order to avoid light leakage towards the Si substrate. Initially, an adhesion layer (Ormoprime) was spun at 4000 rpm for 1 min and baked at $150 \text{ }^\circ\text{C}$ for 5 minutes. Afterwards, diluted Ormocore (Ormocore: thinner maT, 1:2) was spin-coated at 3000 rpm for

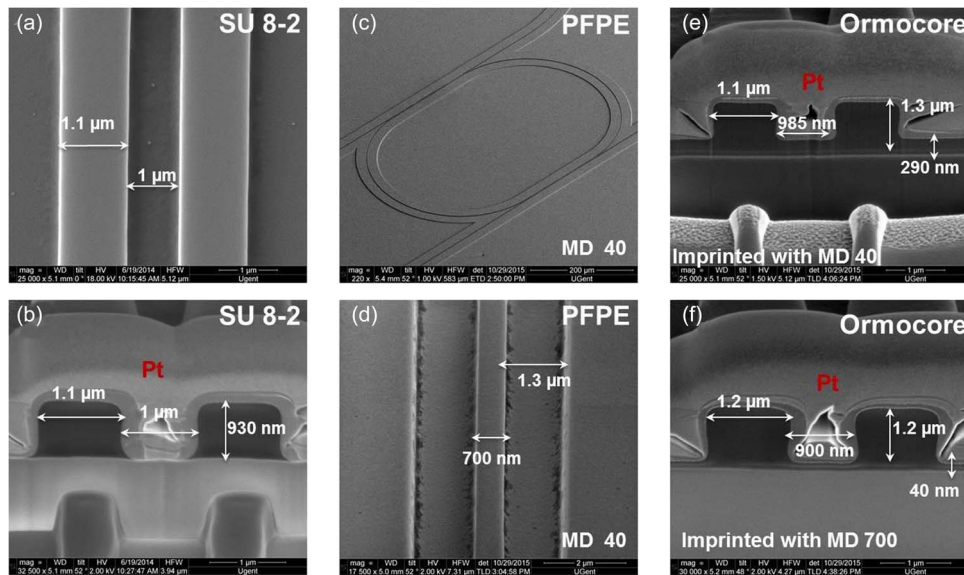


Fig. 2. SEM images of the SU8-2 master mold. (a) Top view. (b) FIB cross section. (c) SEM image of the MRR nanopatterned on PFPE soft mold and (d) its magnification in the gap region. (e) and (f) FIB cross section in the gap region of the imprinted Ormocore microring resonator using MD 40 material and MD 700, respectively.

30 seconds and baked at 120 °C for 10 minutes. The imprinting was done manually by carefully bringing the PFPE composite molds in contact with the Ormocore films at room temperature. Then, 2 minutes of UV illumination with intensity of 30 mW/cm² in a nitrogen atmosphere was applied to UV-cure the Ormocore layer through the mold. Finally, the mold was manually detached and the resulting replicated Ormocore-based microrings were hardened by post-baking for 3 hours at 150 °C. In this regard, Fig. 1(d) shows the final generated Ormocore MRRs after peeling off the PFPE molds.

As already mentioned high Q -factor microrings are desired for many applications. Therefore, there is a particular need to minimize losses in the fabrication process, a.o. by reducing the surface roughness that induced the scattering loss and also the dimensions of the residual layer that influence the bend loss. Fig. 2(a) shows the SEM (scanning electron microscope) images of the fabricated SU8-2 master mold (top image). From the FIB (focused ion beam) cross section in Fig. 2(b), one sees that the SU8 generated pattern has vertical and smooth sidewalls. We have used the Nova 600 Nanolab SEM/FIB device, a dual beam instrument that combines a focused ion beam with an SEM therefore simultaneous imaging of the sample. Ion beam induced material deposition of platinum was used for FIB cross section. The transferred pattern to PFPE composite molds can be seen in Fig. 2(c). It can be observed in the SEM picture with a larger magnification in the gap region (see Fig. 2(d)), that the waveguides dimensions are slightly larger compared to the initial SU8 waveguides therefore resulting in a smaller gap. The final replicated structures in Ormocore [see Fig. 2(e) and (f)], demonstrate that imprinting with MD 40 and MD 700 results in patterns with different dimensions because of different material and physical properties, including Young's modulus, surface tension and surface energy. Therefore the generated patterns have different dimensions in height, width and gap but most importantly there is a huge difference in the resulting residual layer; it is almost seven times smaller for the imprint with MD 700 without applying any further etching process. A residual layer thickness of only 40 nm was obtained at room temperature, without using any extra force in the embossing process and with the Ormocore waveguide being patterned only by the capillary forces. These results clearly demonstrate the importance of choosing the right mold for the right compatible material in the imprinting process flow. We have fabricated centimetre-large areas of microrings with tailored dimensions around 1 μ m width and height, and controlled residual layer

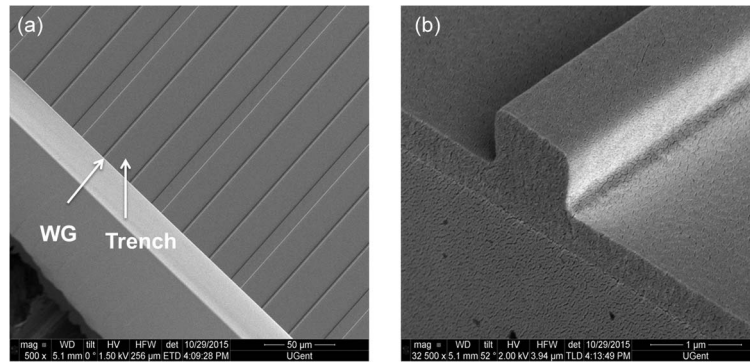


Fig. 3. (a) SEM image of the cleaved Ormocore waveguides. We utilized the “minimum polymer squeezing” method for the reduction of the residual layer on the sides of the ridge shaped waveguide. (b) Sidewall SEM image of the polymer microring imprinted using the MD 40 material.

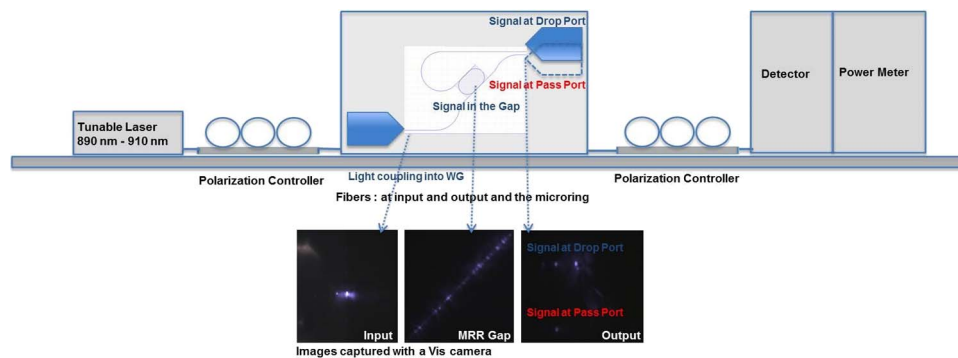


Fig. 4. Schematic of the measurement setup used to characterize the devices. Light from tunable laser sources is coupled into the chip using lensed fiber. The optical microscope pictures show coupling light from a lensed fiber to the waveguide captured with a visible camera, as well as the coupling light in the gap region of the MRR and, moreover, the signal at the pass and drop port.

thickness down to 40 nm. Fig. 3(a) depicts a SEM image of cleaved Ormocore waveguides. In order to minimize the residual layer thickness we adopt the “minimum polymer squeezing” method [20]. The rib-shaped waveguide is generated by imprinting two trenches on both sides of the waveguide, instead of using the single-trench pattern on the mold. As indicated by the arrows in Fig. 3(a), for an almost 1 μm width waveguide, we have 20 μm large trenches. Smooth-sidewall Ormocore waveguides have been fabricated using MD 40 and MD 700. Fig. 3(b) shows a SEM picture of an Ormocore waveguide with good sidewall roughness prepared with MD 40. The transmission spectrum characterization of these devices will be discussed in Section 3.

3. Device Optical Characterization in Transmission Measurements

After fabrication, the polymer MRR transmission spectra were characterized using a tunable laser as a light source (Newport, with a wavelength range: 890–910 nm and 20 pm resolution) and the output signal was measured with a power meter. Fig. 4 shows the horizontal experimental set-up used for the MRR characterization.

The polarization was adjusted by tuning the fiber-based polarization controller. The light is launched into the waveguide through a lensed fiber and collected by another lensed fiber. The coupling of the light into the input waveguide, the light coupled from the bus waveguide into the racetrack microring and finally the output signal at the pass port and the drop port were captured with a visible camera, and shown in Fig. 4 (top view images). According to the simulation

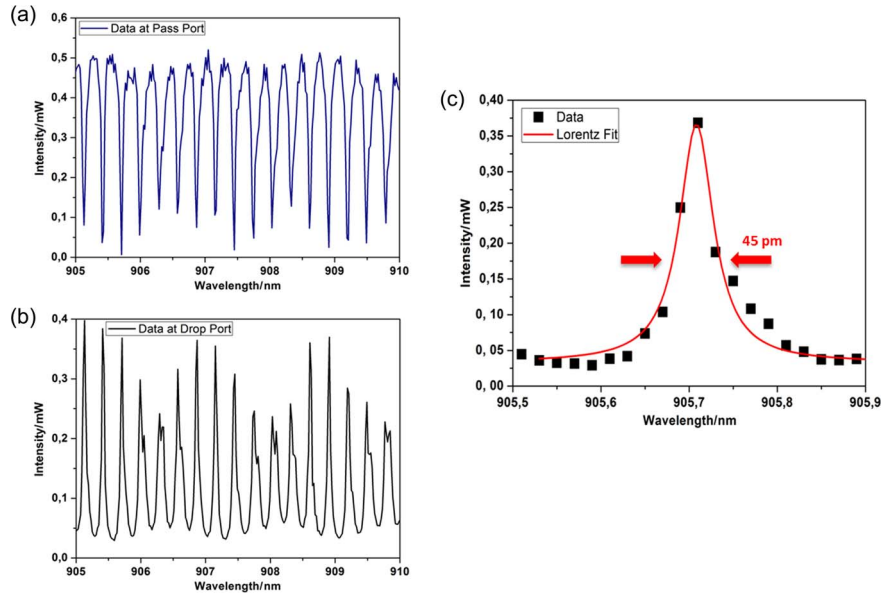


Fig. 5. Optical transmission spectra of the MRRs fabricated with the soft mold using MD 40 measured at (a) the pass port and (b) the drop port, respectively. (c) Lorentzian fit to the resonance peak (solid red line) at the drop port reveals a linewidth of 45 pm corresponding to an optical Q of 20 000.

results, at 890 nm the fabricated waveguides carry both the fundamental TE and TM mode for propagation. However both of the modes have approximately the same effective refractive index, therefore the MRRs have almost the same FSR (free spectral range) for both polarizations. Manually rotating the wheels of the polarization controller, we get a maximum or minimum transmitted power. Therefore, this is a simple way to distinguish TE and TM polarization modes, when knowing which one of them has more loss. We use an add-drop racetrack ring resonator configuration, and therefore, the ring is coupled to two waveguides and therefore the incident field is partly transmitted to the drop port. The transmission to the pass port can be expressed as [21]

$$T_{\text{pass}} = \frac{I_{\text{pass}}}{I_{\text{input}}} = \frac{(r_2 a)^2 - 2r_1 r_2 a \cos \phi + r_1^2}{1 - 2r_1 r_2 a \cos \phi + (r_1 r_2 a)^2}. \quad (1)$$

However, for a symmetric design $r_1 = r_2 = r$ is the field coupling coefficient between the input bus waveguide and the MRR. a , is the amplitude attenuation factor and ϕ is the round trip phase. We can calculate the a and r values based on fitting Lorentzians to the resonances. The amplitude attenuation factor is due to the various optical losses in the microring (including propagation loss, bend loss) and can be used to obtain the $Q_{\text{intrinsic}}$ of the ring with the formula [22], [23]

$$Q_{\text{intrinsic}} = \frac{4\pi^2 R n_{\text{eff}}}{|\ln a| \lambda}. \quad (2)$$

Here, R is the ring radius, n_{eff} is the effective refractive index, and λ is the resonance wavelength. Finally, from $Q_{\text{intrinsic}}$ we can estimate the propagation loss of our devices using the expression $\alpha = 10 \log_{10} e \cdot 2\pi n_g / Q_{\text{int}} \lambda$ where n_g is the group index. Fimmwave software was used to calculate the $n_{\text{eff}} = 1.48$, $n_g = 1.57$, for the devices fabricated using MD 40. The ring radius is 220 μm , and the coupling length 190 μm . The calculated FSR is 0.29 nm.

Fig. 5 depicts the optical transmission spectra of the MRRs fabricated using the soft mold MD 40. One can see that the resonance peaks at the pass port [see Fig. 5(a)] correspond

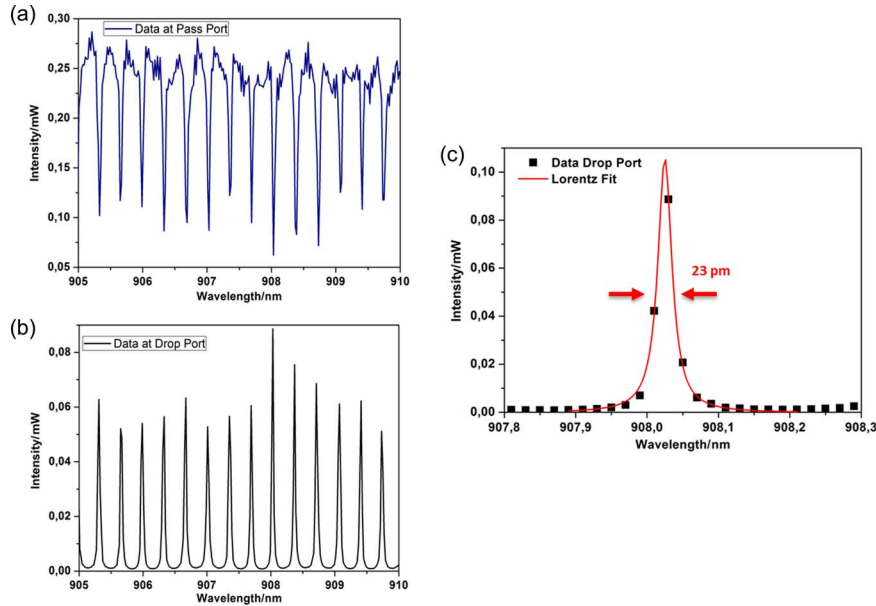


Fig. 6. Optical transmission spectrum of the MRRs fabricated with the soft mold using MD 700 measured at the (a) pass port and (b) the drop port, respectively. (c) Lorentzian fit to the resonance peak (solid red line) at the drop port reveals a linewidth of 23 pm corresponding to an optical Q of 39400.

TABLE 1

Performance comparison of the devices fabricated with MD 40 and MD 700

Device fabricated with:	Q_{total}	F	a	r	$Q_{\text{intrinsic}}$	$\alpha(\text{dB/cm})$
MD 40	20 000	~ 7	0.902	0.827	87 500	5.40
MD 700	39 400	~ 14	0.910	0.943	81 700	5.77

nically to the resonances at the drop port [see Fig. 5(b)]. The estimated FSR is in good agreement with the measurement. The best calculated Q -factor of 20 000 correspond to a linewidth of 45 pm. We find out that the amplitude attenuation factor $a = 0.902$ and the field coupling coefficient $r = 0.827$. The calculated intrinsic factor $Q_{\text{intrinsic}} = 87\,500$ corresponds to the propagation loss of 5.40 dB/cm. The non-uniform extinction ratio in the transmission spectra is due to the large sweeping step of the laser (20 pm) during the measurement.

Fig. 6 shows the optical transmission spectra of the MRRs prepared using MD 700 soft molds on the pass and drop port respectively. In this situation, the MRR has a radius of $180\ \mu\text{m}$ and the same coupling length of $190\ \mu\text{m}$. The calculated $n_{\text{eff}} = 1.48$ and $n_g = 1.58$ lead to a FSR of 0.34 nm. A higher Q -factor of 39 000 corresponding to a linewidth of 23 pm was observed. We find out that the amplitude attenuation factor $a = 0.910$ and the field coupling coefficient $r = 0.943$. The calculated intrinsic factor $Q_{\text{intrinsic}} = 81\,700$ corresponds to a propagation loss of 5.77 dB/cm.

All the calculated parameters are summarized in Table 1. The round trip loss a includes the three loss contributors summarized: $a[\text{dB}] = \alpha L + 2a_{\text{coupler}} + 4a_{\text{bend}}$ [21]. The influence of the waveguide surface roughness on the scattering loss depends on the waveguide geometry and the refractive index contrast between the guiding layer and the surrounding environment. At shorter wavelengths the increase in propagation loss is expected because the surface roughness gives more significant Rayleigh scattering ($\sim 1/\lambda^4$). One can see in Table 1 that the devices prepared with MD 40 have smaller propagation loss compared with those prepared with

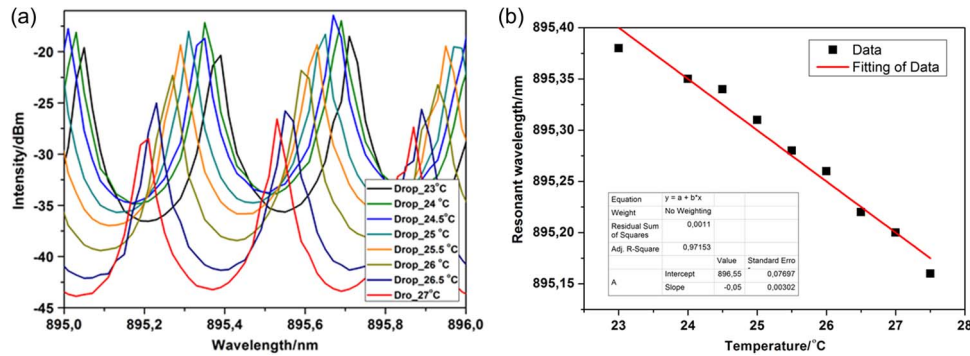


Fig. 7. (a) Temperature sensitivity measurement of the fabricated Ormocore MRR. (b) Linear fitting of the resonant wavelengths at different temperatures.

MD 700. We can understand this, considering that the height of the waveguides prepared with MD 40 is 200 nm smaller than of the waveguides prepared with MD 700 and therefore less material in sidewalls contributes to surface scattering. However, the Q -factor of the devices prepared with MD 700 is almost two times larger than of those prepared with MD 40. This is because the bend losses decrease significantly for the devices prepared with MD 700, having almost seven times smaller residual layer. Because of the racetrack configuration, instead of a ring, additional bend losses appear due to mismatch losses at the straight-bend transition. These losses are more pronounced for MRR with larger residual layers.

T. Ling *et al.* [24] have also reported about the fabrication of polymer MRRs with a high Q factor of 4×10^5 at 780 nm wavelength range. However, in their fabrication process of the master mold, they have used electron beam lithography, which is an expensive technique.

Finally in this study we investigate the temperature-induced resonant wavelength shifts due to the thermo-optic effect in hybrid MRRs. The temperature has been precisely controlled using a temperature controller from 23 °C to 28 °C. Fig. 7(a) depicts the temperature sensitivity measurement of the fabricated Ormocore MRR using the MD 700 mold. From the linear fit of the resonant wavelengths at different temperatures (see Fig. 7(b)) we determine a shift of the resonances of about -0.05 nm/°C. This value is almost four times smaller than the reported values in the literature measured at 1550 nm [25]. However from the expression

$$\frac{d\lambda_m}{dT} = \frac{\lambda_m}{n_{\text{eff}}} \cdot \frac{dn_{\text{eff}}}{dT} + \lambda_m \alpha_{\text{sub}} \quad (3)$$

where α_{sub} is the thermal expansion coefficient of the substrate, one can see that at shorter wavelengths we have a smaller shift in wavelength by changing temperature. Moreover, the refractive index of the material increases with decreasing wavelength.

Temperature is an important issue for biosensing applications. Photonic devices less sensitive to changing in temperature are highly desired [26]. In this context we have demonstrated that working at shorter wavelength is an interesting alternative to solve this inconvenience.

4. Conclusion

In this work, by using a new fabrication process we have successfully produced large areas of hybrid polymer MRRs with very good optical performance at around 890 nm wavelengths. In the nanoimprint process flow we take the advantage of using PFPE composite molds. These molds provide the benefits of both a hard rigid material for high resolution and a soft flexible material for conformable contact without applying pressure. An optimized fabrication process results in MRRs with only 40 nm residual layer and Q -factors of 39 000. Finally, we show that the resonances can be thermo-optically tuned at 0.05 nm/°C at 896 nm, thus demonstrating that at shorter wavelengths the fabricated MRRs are less sensitive to temperature change compared to

at larger wavelengths. Considering that in this spectral range window, cheap light sources are available, and water absorption is much lower than at far infrared wavelengths, we believe that our devices have high potential for many applications including biosensing.

References

- [1] H. Ma, A. K. Y. Jen, and L. R. Dalton, "Polymer-based optical waveguides: Materials, processing, and devices," *Adv. Mater.*, vol. 14, no. 19, pp. 1339–1365, Sep. 2002.
- [2] C.-Y. Chao, W. Fung, and L. J. Guo, "Polymer microring resonators for biochemical applications," *IEEE J. Sel. Topics Quantum Electron.*, vol. 12, no. 1, pp. 134–142, Jan./Feb. 2006.
- [3] J. Jiang *et al.*, "All-polymer photonic devices using excimer laser micromachining," *IEEE Photon. Technol. Lett.*, vol. 16, no. 20, pp. 509–511, Feb. 2004.
- [4] M. H. M. Salleh *et al.*, "Polymer dual ring resonators for label-free optical biosensing using microfluidics," *Chem. Commun.*, vol. 49, pp. 3095–3097, Jan. 2013.
- [5] J. L. Guo, "Nanoimprint lithography: Methods and material requirements," *Adv. Mater.*, vol. 19, no. 4, pp. 495–513, Feb. 2007.
- [6] C. Zhang, S.-L. Chen, T. Ling, and L. J. Guo, "Review of imprinted polymer microrings as ultrasound detectors: Design, fabrication, and characterization," *IEEE Sens. J.*, vol. 15, no. 6, pp. 3241–3248, Jun. 2015.
- [7] S. Y. Chou, P. J. Krauss, and P. J. Renstrom, "Imprint of sub-25 nm vias and trenches in polymers," *Appl. Phys. Lett.*, vol. 67, no. 21, pp. 3114–3119, Sep. 1995.
- [8] J. Hiltunen, M. Hiltunen, J. Puustinen, J. Lappalainen, and P. Karioja, "Fabrication of optical waveguides by imprinting: Usage of positive tone resist as a mould for UV curable polymer," *Opt. Exp.*, vol. 17, no. 25, pp. 22813–22822, Nov. 2009.
- [9] J. Hiltunen, A. Kokkonen, J. Puustinen, M. Hiltunen, and J. Lappalainen, "UV-imprinted single-mode waveguides with low loss at visible wavelength," *IEEE Photon. Technol. Lett.*, vol. 25, no. 10, pp. 996–998, May 2013.
- [10] K. D. Lee *et al.*, "Nanoimprint technology for nano-structured optical devices," *Current Appl. Phys.*, vol. 6, pp. 149–153, Aug. 2006.
- [11] Y. Xia and G. M. Whitesides, "Soft lithography," in *Proc. Annu. Rev. Mater. Sci.*, 1998, vol. 28, pp. 153–184.
- [12] S. S. Williams *et al.*, "High-resolution PFPE-based molding techniques for nanofabrication of high-pattern density, Sub-20 nm features: A fundamental materials approach," *Nano Lett.*, vol. 10, pp. 1421–1428, 2010.
- [13] J. P. Rolland, R. M. V. Dam, D. A. Schorzman, S. R. Quake, and J. M. DeSimone, "Solvent-resistant photocurable 'Liquid Teflon' for microfluidic device fabrication," *J. Amer. Chem. Soc.*, vol. 126, no. 8, pp. 2322–2323, 2004.
- [14] C.-Y. Chao and L. J. Guo, "Biochemical sensors based on polymer microrings with sharp asymmetrical resonance," *Appl. Phys. Lett.*, vol. 83, pp. 1527–1529, 2003.
- [15] M. Hiltunen *et al.*, "Polymeric slot waveguide at visible wavelength," *Opt. Lett.*, vol. 37, no. 21, pp. 4449–4451, Nov. 2012.
- [16] "FIMMWAVE software," Photon Des. Ltd., Oxford, U.K.
- [17] R. Morarescu *et al.*, "Polymer microring resonators for biosensing applications by nanoimprint lithography," in *Proc. IEEE 17th ICTON*, 2015, pp. 1–4.
- [18] *Datasheet forOrmocore, Microresist Technology*. [Online]. Available: <http://www.microresist.de/products/ormocers/pdf/>
- [19] C. Y. Chao and L. J. Guo, "Reduction of surface scattering loss in polymer microrings using thermal-reflow technique," *IEEE Photon. Technol. Lett.*, vol. 16, no. 4, pp. 1498–1500, Jun. 2004.
- [20] T. Han, S. Madden, M. Zhang, R. Charters, and B. L. Davies, "Low loss high index contrast nanoimprinted polysiloxane waveguides," *Opt. Exp.*, vol. 17, no. 4, pp. 2623–2630, 2009.
- [21] W. Bogaerts *et al.*, "Silicon microring resonators," *Laser Photon. Rev.*, vol. 6, no. 1, pp. 47–73, 2012.
- [22] T. Ling, S. L. Chen, and L. J. Guo, "Fabrication and characterization of high Q polymer micro-ring resonator and its application as a sensitive ultrasonic detector," *Opt. Exp.*, vol. 19, no. 2, pp. 861–869, Jan. 2011.
- [23] W. H. P. Pernice, C. Xiong, and H. X. Tang, "High Q micro-ring resonators fabricated from polycrystalline aluminum nitride films for near infrared and visible photonics," *Opt. Exp.*, vol. 20, no. 11, pp. 12261–12269, 2012.
- [24] T. Ling, S. L. Chen, and L. J. Guo, "High-sensitivity and wide-directivity ultrasound detection using high Q polymer microring resonators," *Appl. Phys. Lett.*, vol. 98, 2011, Art. no. 204103.
- [25] D. Rezzonico, A. Guarino, C. Herzog, M. Jazbinsek, and P. Günter, "High-finesse laterally coupled organic-inorganic hybrid polymer microring resonators for VLSI photonics," *IEEE Photon. Technol. Lett.*, vol. 18, no. 7, pp. 865–867, Apr. 2006.
- [26] C. T. Wang *et al.*, "Highly sensitive optical temperature sensor based on a SiN micro-ring resonator with liquid crystal cladding," *Opt. Exp.*, vol. 24, no. 2, pp. 1002–1007, Jan. 2016.